Water Research 181 (2020) 115923

Contents lists available at ScienceDirect

Water Research

journal homepage: www.elsevier.com/locate/watres

Reduced NOM triggered rapid Cr(VI) reduction and formation of NOM-Cr(III) colloids in anoxic environments

Binrui Li [a, b], Peng Liao [b, c, *], Lin Xie [d], Qianqian Li [b], Chao Pan [e], Zigong Ning [b], Chongxuan Liu [b, **]

[a] School of Environment, China University of Geosciences, 388 Lumo Road, Wuhan, 430074, PR China
[b] State Environmental Protection Key Laboratory of Integrated Surface Water-Groundwater Pollution Control, School of Environmental Science and Engineering, Southern University of Science and Technology, Shenzhen, 518055, PR China
[c] State Key Laboratory of Environmental Geochemistry, Institute of Geochemistry, Chinese Academy of Sciences, Guiyang, 550081, PR China
[d] Department of Physics, Southern University of Science and Technology, 1088 Xueyuan Road, Shenzhen, 518055, PR China
[e] Glenn T. Seaborg Institute, Physical & Life Sciences Directorate, Lawrence Livermore National Laboratory, Livermore, CA, 94550, United States

ARTICLE INFO

Article history:
Received 3 January 2020
Received in revised form
31 March 2020
Accepted 6 May 2020
Available online 11 May 2020

Keywords:
Reduced NOM
Cr(VI) reduction rate
Mechanism
NOM-Cr(III) colloid formation
Colloid characterization
Anoxic environments

ABSTRACT

Natural organic matter (NOM) can influence the toxicity and speciation of chromium (Cr) in subsurface through redox reactions and complexation. Under anoxic conditions, NOM can be reduced by microorganisms or geochemical reductants, and the reduced NOM (NOM_{red}) represents a large reservoir of organic matter observed in anoxic sediments and water. While the current body of work has established the kinetic of Cr(VI) reduction by oxidized NOM (NOM_{ox}) under oxic conditions, much less is known about the rates and mechanisms of Cr(VI) reduction triggered by NOM_{red} under anoxic conditions and the colloidal properties of the reaction products. This study provided new information regarding the NOM_{red}-mediated Cr(VI) reduction and colloidal stability of reduced Cr(III) particles over a wide range of environmentally relevant anoxic conditions. We show that under dark anoxic conditions reduced humic acid (HA_{red}) moieties (e.g., quinone) can quickly reduce Cr(VI) to Cr(III), and the reduced Cr(III) can subsequently complex with carboxyl groups of HA leading to the formation of stable HA-Cr(III) colloids. Rates of Cr(VI) reduction by HA_{red} are 3–4 orders of magnitude higher than those by oxidized HA (HA_{ox}) due primarily to the higher reducing capacity of HA_{red}. The stable HA-Cr(III) colloids are formed across a range of HA concentrations (8–150 mg C/L) and pH conditions (6–10) with hydrodynamic diameter in the range of 210–240 nm. Aberration-corrected scanning transmission electron microscopy (Cs-STEM) and X-ray photoelectron spectroscopy (XPS) confirmed that the particles are composed of HA-Cr(III). The high colloidal stability of HA-Cr(III) particles could be attributed to the enhanced electrosteric stabilization effect from free and adsorbed HA, which decreased particle aggregation. However, the presence of divalent cations (Ca^{2+} and Mg^{2+}) promoted particle aggregation at pH 6. These new findings are valuable for our fundamental understanding of the fate and transport of Cr in organic-rich anoxic environments, which also have substantial implications for the development and optimization of subsurface Cr sequestration technology.

1. Introduction

Contamination of groundwater by hexavalent chromium (Cr(VI)) originated from both anthropogenic activities and geochemical processes (e.g., Cr(III) oxidation by manganese oxides) poses a widespread threat to the aquatic ecosystem and drinking water resource (Blowes, 2002; McNeill et al., 2012; McClain et al., 2017). Cr(VI) typically exists as highly mobile oxyanionic species (e.g., $Cr_2O_7^{2-}$, $HCrO_4^-$ and CrO_4^{2-}), whereas Cr(III) is generally considered immobile (Richard and Bourg, 1991). Cr(VI) can be reduced to Cr(III) by a variety of naturally occurring reductants, including Fe(II)-based compounds, sulfide, and natural organic matter (NOM) (Fendorf and Li, 1996; Patterson et al., 1997; Gu and Chen, 2003; Pan et al., 2016). Rates of Cr(VI) reduction by these reductants at concentrations representative of sediment

* Corresponding author. State Environmental Protection Key Laboratory of Integrated Surface Water-Groundwater Pollution Control, School of Environmental Science and Engineering, Southern University of Science and Technology, Shenzhen, 518055, PR China.
** Corresponding author.
E-mail addresses: liaop@sustech.edu.cn (P. Liao), liucx@sustech.edu.cn (C. Liu).

https://doi.org/10.1016/j.watres.2020.115923
0043-1354/

porewaters have been found to span five orders of magnitude (Graham and Bouwer, 2010). Reduced Cr(III) products can be (1) precipitated as pure $Cr(OH)_3$ solids or a mixed Cr(III)–Fe(III)-(oxy) hydroxide solid solution (Eary and Rai, 1988) or (2) complexed with organic ligands as a mobile Cr(III) phase (James and Bartlett, 1983). Knowledge of both the rate of Cr(VI) reduction and particle stability of reduced Cr(III) products are important for assessing the ultimate fate of Cr in subsurface environments.

NOM is a chemically heterogeneous mixture of redox-active organic macromolecules that occur widely in subsurface environments and can modulate the redox chemistry of redox-sensitive metals (Aiken, 1985; Stevenson, 1994; Aiken et al., 2011). NOM can reduce Cr(VI) over a wide pH range (e.g., 2–7) under oxic conditions (Wittbrodt and Palmer, 1995, 1996; Nakayasu et al., 1999). The rate of Cr(VI) reduction by NOM at circumneutral pH was on the order of weeks to months (Wittbrodt and Palmer, 1995). In addition to direct reduction of Cr(VI), NOM could also influence Cr(VI) reduction by Fe(II) under oxic conditions. For example, NOM was found to accelerate or inhibit the rate of Cr(VI) reduction by Fe(II), and the extent of acceleration or inhibition was dependent on pH (Buerge and Hug, 1998; Pan et al., 2017a).

Although a large body of previous researches have provided valuable insights on the interactions between Cr(VI) and NOM (Wittbrodt and Palmer, 1995, 1996), most studies have focused on the reduction of Cr(VI) by oxidized NOM (NOM_{ox}) under oxic conditions, and there is little work devoted to understanding the kinetic and mechanism of Cr(VI) reduction by reduced NOM (NOM_{red}) under anoxic conditions. Depending on redox conditions, NOM can exist either as an oxidized or a reduced state (Aeschbacher et al., 2010). Under anoxic conditions, NOM can be reduced by a variety of microorganisms (e.g., fermenting, iron-, and sulfate-reducing bacteria) and geochemical reducing species (e.g., sulfide) (Lovley et al., 1996; Coates et al., 1998; Gu et al., 2011). Quinone-hydroquinone pairs have been recognized as the principal reducible moieties present in NOM_{red} (Scott et al., 1998). NOM_{red} can serve as an important electron donor and, thus, participate in multiple redox reactions that affect the biogeochemical redox transformation of redox-active metals (e.g., Fe(III) and Hg(II)) and organic pollutants (Lovley and Anderson, 2000; Kappler and Haderlein, 2003; Zheng et al., 2012). A mechanistic and quantitative understanding of Cr(VI) reduction by the chemically active groups of NOM_{red} is critical for a thorough estimation of the cycling of Cr in anoxic subsurface environments.

In addition to interacting with Cr(VI), NOM can complex with reduced Cr(III) products, which is important for the speciation, solubility and mobility of Cr (Kaczynski and Kieber, 1994; Puzon et al., 2008; Gustafsson et al., 2014). Although reduced Cr(III) has been thought to be an important sink of Cr (Liu et al., 2017), laboratory studies have demonstrated that bacterial and organic reduction of Cr(VI) can result in organically complexed Cr(III) that can remain in water for a relatively long period of time (James and Bartlett, 1983; Puzon et al., 2005, 2008). Evidence from field studies further demonstrated that organically complexed Cr(III) constitutes a large fraction (e.g., 25–90%) of the total Cr pool in a wide range of environments (Icopini and Long, 2002; Hu et al., 2016). As the particle size of NOM belong typically to the colloidal size fraction (e.g., 1–220 nm) (Sharma et al., 2010; Liao et al., 2017a), NOM-Cr(III) complexes may exist in a colloidal form (Pan et al., 2017a). The formation of colloidal NOM-metals (e.g., Fe(III) and Mn(III)) has the potential to enhance the mobility of metals in subsurface environments (Pokrovsky and Schott, 2002; Li et al., 2019). Because the mobility of NOM-Cr(III) colloids could lead to concerns of Cr(III) reoxidation, it is important to have a detailed understanding of the formation and properties of NOM-Cr(III) colloids upon Cr(VI) reduction by NOM_{red}. Although the stabilization of soluble Cr(III) by NOM has been recognized (Puzon et al., 2005; Sander and Koschinsky, 2011), there has been no attempt to fundamentally characterize the properties of colloidal Cr(III) particles complexed by NOM_{red} under anoxic conditions.

The objective of this study was to provide new insights into the NOM_{red}-mediated Cr(VI) reduction and NOM-Cr(III) colloid formation in anoxic environments over a range of relevant water chemistry conditions using chemically reduced NOM of different origins. Batch experiments were used to systematically investigate the effect of NOM concentration, pH, ionic strength, and common cations (Na^+, Ca^{2+}, and Mg^{2+}) on the rates and mechanisms of Cr(VI) reduction and the formation and colloidal stability of NOM-Cr(III) colloids under anoxic conditions. Colloids generated in batch experiments were fundamentally characterized using a suite of analytical techniques that provided molecular and nanoscale insights into the properties (e.g., particle size, zeta potentials, surface chemistry, and morphology) of NOM-Cr(III) colloids. Results suggest that formation of stable NOM-Cr(III) colloids upon reduction of Cr(VI) by NOM_{red} represents a potential pathway for Cr(III) transport in organic-rich anoxic environments.

2. Materials and methods

2.1. NOM isolation and characterization

NOM isolates used in this study included a technical Aldrich humic acid (AHA, 1415-93-6) obtained from Sigma-Aldrich and a Pahokee Peat soil humic acid (PPSHA, 2BS103P) obtained from the International Humic Substances Society (IHSS). Both HA isolates were selected as they are well-characterized and have been extensively used for studying NOM-metals interactions (Liu et al., 2011; Liao et al., 2017a; Pan et al., 2017a). Stock suspensions of each HA isolate were filtrated through 0.45 μm nitrocellulose membranes (Millipore) under a vacuum, and referred to as oxidized HAs (AHA_{ox} and $PPSHA_{ox}$). To emulate the HA reduced state occurring in anoxic conditions, aliquots of these oxidized HA suspensions were chemically reduced using 5% H_2 in the presence of a Pd catalyst (5% wt on Al_2O_3 spheres, 1 g/L, Sigma-Aldrich) in an anoxic glovebox (95% N_2 and 5% H_2, Coy Laboratory Products Inc., MI) as described previously (Liao et al., 2017b, 2019). The resulting suspensions were referred to as reduced HAs (AHA_{red} and $PPSHA_{red}$). Stock suspensions of both oxidized and reduced HAs were stored in an anoxic glovebox in the dark before use.

Concentrations of HA were determined using a total organic carbon (TOC) analyzer (Multi N/C 3100, Analytik Jena). The Fe content for each HA was determined using the method presented by Lovley and Blunt-Harris (1999). The redox capacity of HAs was quantified following a modified procedure described by Lovely et al. (1996). Briefly, 5 mM Fe(III) citrate was mixed with an aliquot of HA stock suspensions and then allowed to equilibrate on a rotator for 1 h before an aliquot was taken for Fe(II) determination using a 1,10-phenanthroline assay described previously (Tamura et al., 1974). The electron-carrying capacity of each HA was determined as the difference between the Fe(II) concentration of the reduced and oxidized HA samples. Additional information, including elemental composition, ^{13}C nuclear magnetic resonance (NMR), and specific ultraviolet absorbance ($SUVA_{254}$), are given elsewhere (Liao et al., 2017a, 2019; Li et al., 2019); a summary is also provided in Table S1 in the Supplementary Material.

2.2. Batch experiments

The batch experimental conditions are summarized in Table S2. All batch experiments were performed in 50-mL capped polypropylene bottles that were continuously stirred with Teflon-

coated magnetic stir bars at a speed of 650 rpm and were maintained at a constant temperature (25 ± 0.5 °C) inside the anoxic glovebox. The reactors were shielded with aluminum foil to exclude any photochemical reactions. All experiments and sample preparations were conducted inside an anoxic glovebox with less than 0.1 ppm of gaseous O_2. All solutions and reagents were made in the anaerobic chamber using deoxygenated water, which was prepared by sparging ultrapure water with ultrapure N_2 for 4 h, and then equilibrating with the anoxic atmosphere in the chamber for at least 12 h. A Cr(VI) stock solution (0.1 g/L) was prepared from $K_2Cr_2O_7$. For most experiments, the pH of the reaction suspension was maintained at pH 6 using 5 mM 2-morpholinoethansulfonic acid monohydrate (MES, Sigma-Aldrich) buffer. For selected experiments, 5 mM N, *N*′-diethylpiperazine (DEPP, Sigma-Aldrich) was used as the buffer for pH 5.0; 5 mM 4-(2-hydroxyethyl)-1-piperazineethanesulfonic acid (HEPES, Sigma-Aldrich) was used for pH 7 and 8; 5 mM *N*-Cyclohexyl-2-aminoethanesulfonic acid (CHES, Sigma-Aldrich) for pH 9; and 5 mM *N*-cyclohexyl-3-aminopropanesulfonic acid (CAPS, Sigma-Aldrich) for pH 10. These pH buffers were selected because they are non-complexing agents that have been widely used to study Cr redox reactions (Wadhawan et al., 2013; Pan et al., 2017a). A constant background ionic strength was maintained by the 5 mM buffers without the addition of any other electrolytes.

Reactions were initiated by adding 1 mg/L Cr(VI) from the stock solution to a vigorously stirred solution containing HA_{red} (AHA_{red} and $PPSHA_{red}$) working suspension at concentrations ranging from 0–150 mg C/L and 5 mM MES (pH 6) in an anoxic glovebox. The dissolved oxygen concentrations in the suspensions were below the detection limit (0.01 mg/L) of the DO probe throughout the course of experiment periods. Separate control experiments with HA_{ox} (80 mg C/L AHA_{ox} and 150 mg C/L $PPSHA_{ox}$) were conducted under identical conditions as described above. Additional experiments with a fixed AHA_{red} of 40 mg C/L were performed to evaluate the effects of pH (5–10), ionic strength (0.5–100 mM) and composition (NaCl, $CaCl_2$, and $MgCl_2$) on the kinetics of Cr(VI) reduction and colloidal stability of formed Cr(III) products at pH 6. The effect of multiple Cr(VI) spikes was also investigated in separate experiments. The experiments involved spiking 1 mg/L Cr(VI) with 80 mg C/L AHA_{red} at pH 6 and monitoring Cr(VI) concentration evolution over time. Once there was no detectable Cr(VI) remaining in the suspension, another spike of Cr(VI) was added. All other experimental conditions were the same as those used for the initial experiments described above.

Suspension aliquots were periodically collected from each batch reactor at desired time intervals using a 2 mL polypropylene syringe. Subsamples of ~1 mL were filtered using a 0.22 μm syringe filter (PES, Millipore) and the filtrate was analyzed immediately for aqueous Cr(VI) and total aqueous Cr. The remaining sample in the syringe was dispensed as an unfiltered suspension and used for total Cr analyses. Samples for measurement of total aqueous Cr and total Cr were acidified in 4% HNO_3 and stored at 4 °C in the dark.

2.3. Aqueous and solid phase analysis

Cr(VI) concentrations in the samples were measured spectrophotometrically using a diphenyl carbazide (DPC) method at a wavelength of 540 nm. Total aqueous Cr and total Cr concentrations were determined using an Agilent 7700 series inductively coupled plasma mass spectrometry (ICP-MS). Cr(III) concentrations were quantified as the difference between total Cr and Cr(VI) concentrations. Truly dissolved (<10000 Da, roughly equal to <1–3 nm), colloidal (10000 Da–220 nm), and particulate (>220 nm) Cr (Cr(VI) and Cr(III)) were fractionated from samples collected at the end of each batch experiment using 10 kDa ultrafiltration (EMD, Millipore) and 0.22 μm filtration (PES, Millipore). In this study, colloids were defined as particles ranging from 10000 Da to 220 nm.

The particle size and zeta potential of the suspensions collected after Cr(VI) reduction were probed by dynamic light scattering (DLS) using a Zetasizer Nano (Malvern Instruments). Scanning transmission electron microscopy (STEM) samples collected after Cr(VI) reduction were prepared by depositing ~10 μL of suspension onto a 10-nm thick window of silicon nitride membrane (SN100, SiMPore Inc, USA) followed by evaporation of the remaining water with deoxygenated gas inside the glovebox. Particles were imaged using an ultrahigh-resolution double-spherical aberration-corrected STEM at 300 kV (Cs-corrected STEM, Thermo Fisher, Titan Themis G2 60e300). Details of STEM and energy dispersive X-ray (EDX) measurements can be found in our previous publication (Li et al., 2019).

The surface properties of the resulting Cr(III) products were characterized by attenuated total reflectance Fourier transform infrared (ATR-FTIR) spectroscopy and X-ray photoelectron spectroscopy (XPS). Solid samples were prepared by centrifugation and then freeze-dried under anoxic conditions. ATR-FTIR spectra were recorded using a Thermo Nicolet iS50 FT-IR spectrometer equipped with a diamond internal reflection element (IRE). Samples were prepared on the ATR cell by placing the freeze-dried solids evenly onto the diamond crystal surface with a diameter of ~3 mm under an argon environment. A dry cell purged with argon gas was used as a background for all sample. Data were collected over the 4000–500 cm^{-1} range at a resolution of 4 cm^{-1}. Spectra were proceeded using the OMNIC software package. XPS spectra were collected using a PHI Quantera SXM scanning X-ray microprobe with an Al mono source at a 100 μm X-ray spot size. The binding energies were calibrated using C 1s at 284.8 eV and the spectra were proceeded using MultiPak v9.8 software.

2.4. Data analysis

An empirical pseudofirst-order rate law proposed by Zheng et al. (2012) was employed to simulate the reduction of Cr(VI) by HA_{red} in this study. The model was established with the assumption that Cr(VI) reduction undergoes multiple pathways involving different functional groups with different reactivities (see discussion below). The pseudofirst-order kinetic model can be described using the following parallel reactions:

$$Cr(VI)_1 + reductant_1 \xrightarrow{k_1} Cr(III) \quad (1)$$

$$Cr(VI)_2 + reductant_2 \xrightarrow{k_2} Cr(III) \quad (2)$$

where reductants 1 and 2 represent different types of reducing moieties or reactive sites in HA_{red}. Combining equations (1) and (2) yields:

$$-\frac{[Cr(VI)]}{[Cr(VI)]_0} = A \cdot exp^{(-k_1 t)} + (1-A) \cdot exp^{(-k_2 t)} \quad (3)$$

where A and 1–A are fractions of HA_{red} reacted with Cr(VI) with rate constants of k_1 and k_2, respectively, which can be determined by fitting the experimental data using a nonlinear least-squares algorithm.

3. Results and discussion

3.1. Reduction of Cr(VI) by NOM_{red}

The result from anoxic batch experiments indicated that HA_{red} is a potent reductant of Cr(VI) at the near-neutral pH 6 (Fig. 1a). HA-free

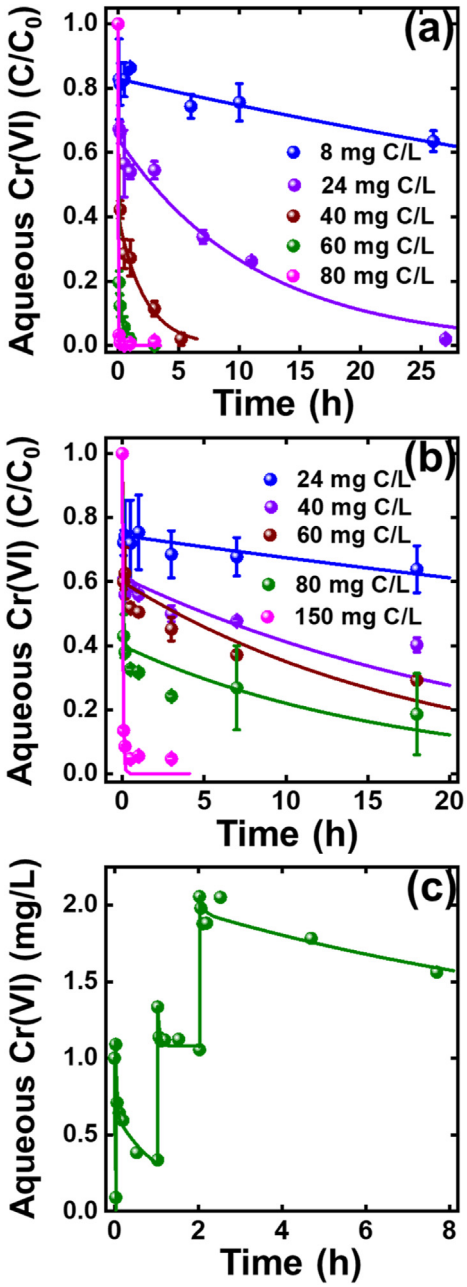

Fig. 1. Reduction of Cr(VI) by (a) AHA_{red} and (b) $PPSHA_{red}$ under anoxic conditions at pH 6. (c) Reduction of Cr(VI) by AHA_{red} for the multiple spiking experiments under anoxic conditions at pH 6. The AHA_{red} concentration was fixed at 40 mg C/L. Spiking of Cr(VI) (each 1 mg/L) when Cr(VI) concentration decreased to below detection started another Cr(VI) reduction experiment. Aqueous Cr(VI) concentration was determined after filtration through a 0.22 μm PES syringe filter. Solid lines represent the pseudofirst-order model fits using equation (3). Error bars represent the standard deviations of at least duplicate measurements. Where error bars are not visible, they are smaller than the data symbols.

control experiments showed no Cr(VI) reduction by Pd/H_2 treated solution in the glovebox over the duration of the experiments (not shown), suggesting that reductants other than HA are absent. Although oxidized HA (or fulvic acid) was previously reported to initiate Cr(VI) reduction (Wittbrodt and Palmer, 1995), this was not obvious at pH 6 (Fig. S1), likely due to the time needed to reduce Cr(VI) (weeks to months) significantly longer than the time of 27 h used in this study. In contrast, the reduction of Cr(VI) by HA_{red} is rapid with rates on a time scale of minutes (k_1 = 0.36–0.72 min^{-1}, Fig. 1a and b, Table S2). Rates of Cr(VI) reduction by HA_{red} (AHA_{red} and $PPSHA_{red}$) are 3–4 orders of magnitude higher than those by HA_{ox} (Fig. S1, Table S2) primarily due to the higher reducing capacity of HA_{red} (Jiang and Kappler, 2008). This is consistent with previous observations that HA_{red} is much more reactive than HA_{ox} for mediating Fe(III) and Hg(II) reduction under anoxic conditions (Gu et al., 2011; Zheng et al., 2012; Liao et al., 2017b). Concentrations of intrinsic Fe(II) (0.06–3.6 μM) present in HA_{red} working suspensions were much lower than the added Cr(VI) concentration (17.8 μM) and, thus, the contribution of intrinsic Fe(II) to the observed Cr(VI) reduction appears negligible. For both AHA_{red} and $PPSHA_{red}$, the extent of Cr(VI) reduction increased with increasing initial HA_{red} concentration (Fig. 1a and b), which supports our contention that increasing HA_{red} concentration would lead to an increase in the concentration of redox-active functional groups available for Cr(VI) reduction. This is first direct quantification of the rates of Cr(VI) reduction by HA_{red} under conditions relevant to anoxic subsurface environments.

Cr(VI) reduction by HA_{red} may undergo several pathways that involve multiple types of redox-active sites with different reactivities. Evidence from previous studies suggested that two quinone-like structures (Q_1 and Q_2) and a non-quinone structure accounted for the total electron-carrying capacity of HA_{red} (Ratasuk and Nanny, 2007). Q_1 is referred as quinone moieties have a neighboring electron-withdrawing group, while Q_2 contains either no substituents near the quinone or had nearby electron-donating groups with substituents (Ratasuk and Nanny, 2007). For both AHA_{red} and $PPSHA_{red}$, aqueous Cr(VI) concentrations decreased quickly within the first 30 min and then dropped slowly until a steady-state is attained (Fig. 1a and b). A two-site pseudofirst-order rate model (equation (3)) effectively described the reduction of Cr(VI) by HA_{red} under all conditions tested ($R^2 > 0.93$). At conditions similar to ours (pH 7, anoxic), Zheng et al. (2012) reported that the same two-site model could also simulate the dynamics of Hg(II) reduction by NOM_{red}. The initial rapid drop in Cr(VI) concentrations that we observed is likely caused by reduced quinone sites (Q_1 and Q_2), because quinones have been identified as the principal reducible moieties in HA with reactivities much higher than the bulk of reduction sites in HA (Scott et al., 1998; Jiang and Kappler, 2008; Aeschbacher et al., 2010). The subsequently slow Cr(VI) reduction (k_2 = 0.009–0.457 h^{-1}, Table S2) may have been controlled by non-quinone compounds (e.g., thiol or bisulfide), which accounted for a minor fraction of the electrons that may be transferred from HA_{red} to Cr(VI).

For a given HA_{red} concentration, AHA_{red} is found to be more effective than $PPASH_{red}$ in reducing Cr(VI) (Fig. 1a and b). These observations could be attributed to the different chemical and functional properties of HA of different origins. Table S1 shows that AHA had a higher electron-carrying capacity (3895 ± 448 vs 2216 ± 229 μeq/gC) and a larger amount of organically bound sulfur (3.5 vs 0.6%) compared to PPASH. Thus, the higher density of the redox-active functional groups (e.g., quinone-like moieties) and reduced forms of sulfur (non-quinone structure) in AHA are likely responsible for the observed higher extent and rate of Cr(VI) reduction by AHA_{red}. Multiple spiking experiments showed a decrease in Cr(VI) reduction with each successive Cr(VI) spike (Fig. 1c). However, the rate after the forth Cr(VI) spike was still 4 orders of magnitude higher than the rate of Cr(VI) reduction by HA_{ox} ($k_1 = 1.67 \times 10^{-1}$ versus 5.83×10^{-5} min^{-1}), suggesting that a portion of the redox-active moieties in HA persisted and could further donate electrons to Cr(VI). This is similar to previous observations that the reduced moieties in HA_{red} had not been completely oxidized during oxygenation events (Bauer and Kappler, 2009).

3.2. Effect of pH and common cations on Cr(VI) reduction

Cr(VI) reduction by AHA_{red} is faster at lower pH and generally decreases with increasing pH (Fig. 2a). For example, at a loading of 40 mg C/L AHA_{red}, ~80% Cr(VI) reduction occurred within 30 min at pH 5, whereas only 48% Cr(VI) reduction was observed at pH 10 after 3 h (Fig. 2a). This pH-dependence of Cr(VI) reduction is consistent with earlier reports showing that the rate of Cr(VI) reduction by NOM decreased with increasing pH from 2 to 7 under oxic conditions (Wittbrodt and Palmer, 1995). An increase in pH could lower the reduction potential of the Cr(VI)/Cr(III) half reaction (Lide, 2000); thus Cr(VI) could be a weaker oxidant at higher pH. Further, carboxyl groups of HA can introduce negative charge with increased density with increasing pH (Fig. S2). Lower Cr(VI) reduction at higher pH might be due to the stronger unfavorable electrostatic interactions between negatively charged Cr(VI) ($pK_a = 0.74$; $pK_b = 6.50$) and HA, which could lead to a higher activation energy, slowing down the electron transfer reactions between HA_{red} and Cr(VI) (Gu and Chen, 2003). At pH 7 the rate of Cr(VI) reduction was slightly higher than at pH 6 (Fig. 2a, Table S2). This deviation of the general trend of Cr(VI) reduction versus pH was probably attributed to the higher reactivity of quinones available for Cr(VI) reduction at pH 7 (Lian et al., 2016).

The presence of common cations (Na^+, Ca^{2+}, and Mg^{2+}) enhanced the reduction of Cr(VI) by AHA_{red} (Fig. 2b–d). The extent and rate of Cr(VI) reduction increased with increasing Na^+ concentration (Fig. 2b). Ca^{2+} and Mg^{2+} also promoted Cr(VI) reduction, but the greatest increases in the reduction rate occurred at lower concentrations (i.e., 0.5 mM Ca^{2+}/Mg^{2+}, Fig. 2c and d). Divalent cations (Ca^{2+} and Mg^{2+}) could bind with the carboxyl groups of HA through complexation reactions that affect the HA surface charge and binding sites for other competing metal ions (Hering and Morel, 1988; Wall and Choppin, 2003; Liao et al., 2019). Zeta potential measurements showed that all three cations lowered the negative charge of HA, but divalent Ca^{2+} and Mg^{2+} had much more pronounced effects for neutralizing HA's negative surface charge than monovalent Na^+ (Figs. S3 and S4). Sorption of anionic Cr(VI) to HA is thus less electrostatically unfavorable and may contribute to the observed rates of Cr(VI) reduction. Liao et al. (2019) reported an inhibitory effect of Ca^{2+} and Mg^{2+} on the redox reactivity of HA and attributed it to the complexation and aggregation of HA by Ca^{2+} and Mg^{2+} that blocked the active site of HA and suppressed the electron transfer reactions. The promotional effect of Ca^{2+} and Mg^{2+} on Cr(VI) reduction by HA_{red} observed in this study suggested that the redox-active groups (e.g., quinone and sulfur-containing sites) may not be influenced by Ca^{2+} and Mg^{2+}, and that the reduction of Cr(VI) by the redox-active groups was much faster than the aggregation of HA by Ca^{2+} and Mg^{2+} at concentrations (0.5–10 mM) tested in this study.

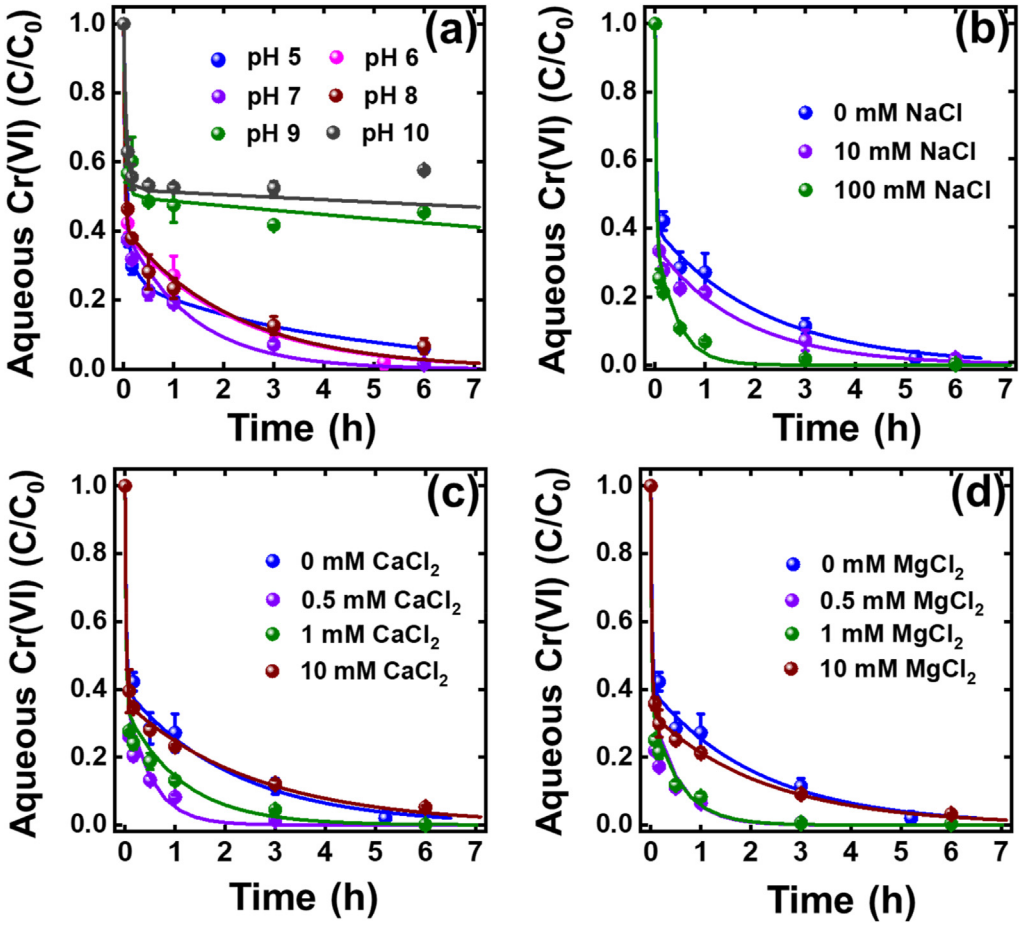

Fig. 2. (a) Effects of pH on the reduction of Cr(VI) by AHA_{red} under anoxic conditions. (b,c,d) Effect of (b) NaCl, (c) $CaCl_2$, and (d) $MgCl_2$ concentrations on the reduction of Cr(VI) by AHA_{red} under anoxic conditions at pH 6. The AHA_{red} concentration was fixed at 40 mg C/L. Aqueous Cr(VI) concentration was determined after filtration through a 0.22 μm PES syringe filter. Solid lines represent the pseudofirst-order model fits using equation (3). Error bars represent the standard deviations of at least duplicate measurements. Where error bars are not visible, they are smaller than the data symbols.

3.3. Formation of NOM-Cr(III) colloids upon Cr(VI) reduction

Cr(VI) reduction by HA_{red} is accompanied by colloidal Cr(III) formation. Even when Cr(VI) concentration dropped to a very low concentration, we still need to consider the particle stability of reduced Cr(III) because Cr(III) species could be reoxidized to toxic Cr(VI) when they are exposed to oxidizing conditions (Landrot et al., 2012). Concentrations of Cr(III) observed in suspensions appeared to correlate with the rate of Cr(VI) reduction (Figs. S5 and S6). For all experiments, the aqueous Cr(III) (<220 nm) and total Cr(III) concentrations rose rapidly within the first 30 min and then gradually approached a plateau (Figs. S5 and S6). The ratio of aqueous Cr(III) to total Cr(III) was observed to be > 0.87 for all HA concentration conditions, suggesting that aqueous Cr(III) dominated. Further size partitioning results clearly demonstrated that truly dissolved Cr(III) (<1–3 nm) was negligible after 10 kDa membrane ultrafiltration, and most of Cr(III) was present in colloidal form (10000 Da–220 nm) (Fig. 3a and b). In contrast to Cr(III), the remaining Cr(VI) after reduction was primarily present as truly dissolved form with Cr(VI) concentrations in the filtered fraction (<10000 Da) being quite high (Fig. S7). Colloidal Cr(III) constituted as much as 80–99% of the total Cr(III) fraction in the suspensions, regardless of the concentration and origin of HA (Fig. 3a and b). This is similar to prior work of Wu et al. (2001) who reported that substantial portions (99%) of the operationally defined dissolved metal (e.g., Fe(III)) were present in colloidal phase in marine environments.

Formation of HA-Cr(III) colloids is likely due to the complexation of Cr(III) with HA followed by polymerization of HA. Although Cr(III) has a low solubility at neutral pH (e.g., 10^{-9} M, Sass and Rai, 1987), the measured colloidal Cr(III) concentrations in this study were much higher than the predicted solubility of $Cr(OH)_3(s)$, which may be ascribed to the formation of HA-Cr(III) complexes (Kaczynski and Kieber, 1994; Fukushima et al., 1995). Complexation of Cr(III) by HA may inhibit extensive hydrolysis of Cr(III) to $Cr(OH)_3$ and thus inhibit particle aggregation to favor smaller particle sizes (Kaczynski and Kieber, 1994; Icopini and Long, 2002). DLS results support this proposition, showing that the hydrodynamic diameters of suspensions were in the range of 210–240 nm (Fig. 3c and d) and remained largely unchanged over 60 days. Zeta potential measurements provided further evidence for the colloidal stabilization of HA-Cr(III) complexes. The zeta potentials of suspensions for all HA concentration conditions show significant negative surface charges (−41.2 ~ −49.1 mV, Fig. 3c and d), supporting the observed high dispersion of HA-Cr(III) colloids due to strong electrostatic stabilization effect from free HA adsorbed on the surfaces of colloids (Liao et al., 2017a; Pan et al., 2017a). This stabilization mechanism has also been observed for the formation of HA-Fe(III) colloids (Liao et al., 2017a).

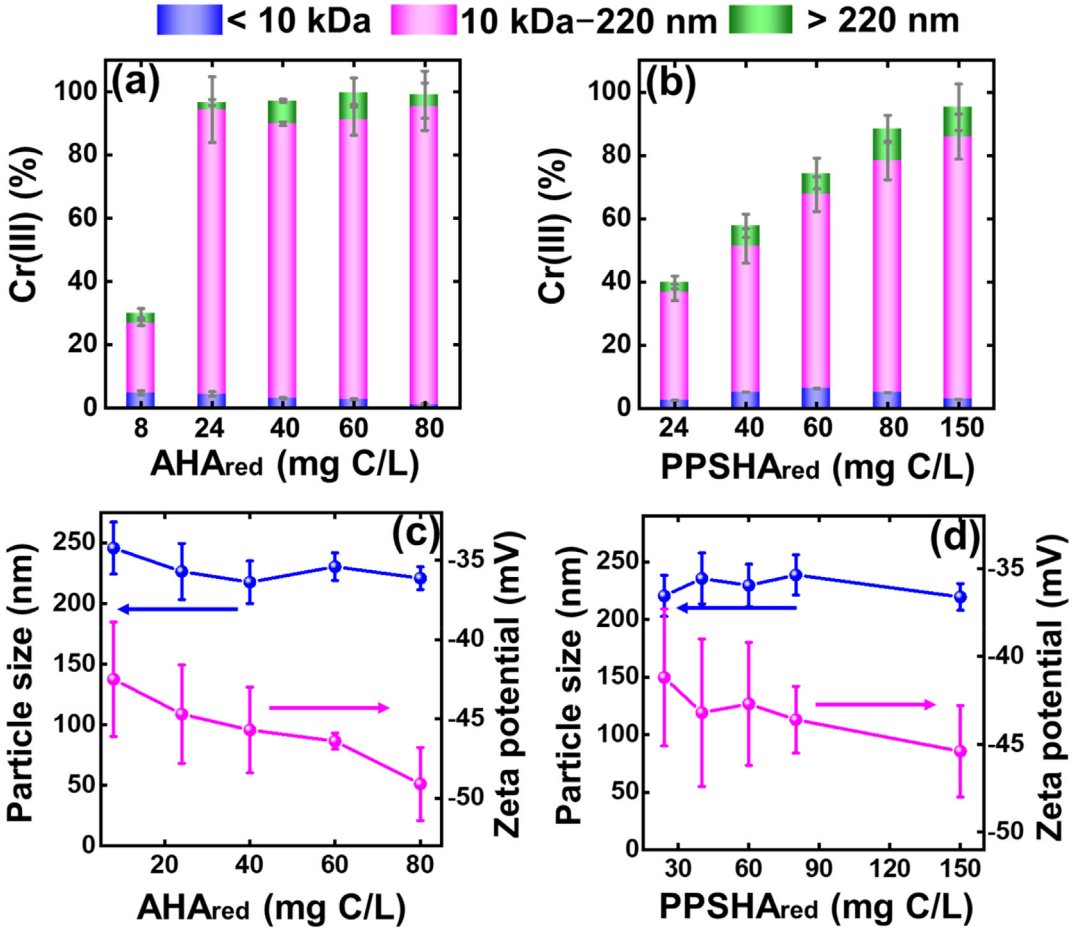

Fig. 3. (a,b) Percentage of Cr(III) concentrations after Cr(VI) reduction in different size fractions under anoxic steady-state conditions as a function of initial (a) AHA_{red} and (b) $PPSHA_{red}$ concentrations. The percentage in y-axis represents the concentration of Cr(III) in a certain size fraction to the total concentration of Cr in the suspension. (c,d) Z-averaged hydrodynamic diameter and zeta potential of HA-Cr suspensions after Cr(VI) reduction under anoxic steady-state conditions as a function of initial (c) AHA_{red} and (d) $PPSHA_{red}$ concentrations. Error bars represent the standard deviations of at least duplicate measurements. Where error bars are not visible, they are smaller than the data symbols.

pH had a marginal influence on the formation and colloidal stability of HA-Cr(III) colloids (Fig. 4a and b). An increase in pH from 6 to 10 did not significantly alter the size fractionation of Cr(III), and colloidal Cr(III) remained the dominant Cr(III) fraction (Fig. 4a). This is consistent with DLS results (Fig. 4b), which showed that the hydrodynamic diameters of suspensions were comparable (217–261 nm) at pH 6–10. This is because the formed HA-Cr(III) colloids under these conditions were highly negatively charged (−45.7 ~ −72.2 mV, Fig. S2), resulting in strong electrostatic repulsive forces between particles and thus preventing their aggregation. In contrast, the zeta potential of the suspensions at pH 5 was −27.2 mV, a value near the typical threshold of −30 mV via Derjaguin-Landau-Verwey-Overbeek (DLVO) theory (Elimelech et al., 1995), and consequently, aggregation of HA-Cr(III) colloids to larger particles could occur readily. This is confirmed by the relatively low colloidal Cr(III) concentration and larger hydrodynamic diameter of suspensions at pH 5 (Fig. 4a and b).

Divalent cations (Ca^{2+} and Mg^{2+}) affected the HA-Cr(III) colloids formation in a concentration-dependent manner (Fig. 4e–h). At $Ca^{2+}/Mg^{2+} \leq 1$ mM, the HA-Cr(III) suspensions were colloidal stable. However, a substantial decrease in colloidal Cr(III) concentration and increase in particle size were observed as the Ca^{2+}/Mg^{2+} concentrations increased from 1 to 10 mM (Fig. 4e–h). The aggregation and destabilization of HA-Cr(III) colloids at higher Ca^{2+} and Mg^{2+} concentrations can be explained by electrostatic interactions through DLVO theory (Elimelech et al., 1995). Zeta potential results showed a dramatic drop in surface negative charge as a function of increasing Ca^{2+} and Mg^{2+} concentrations (Fig. S4). For example, at 10 mM Ca^{2+}/Mg^{2+}, the HA-Cr(III) suspensions were only slightly negatively charged, being −14 ± 0.8 mV for Ca^{2+} and −16.8 ± 2.4 mV for Mg^{2+}, leading to very weak repulsive energy between particles and thus accelerating particle aggregation. The extent of the decrease in colloidal Cr(III) concentrations due to aggregation was more pronounced for Ca^{2+} than for Mg^{2+} (Fig. 4e–h), likely due to the stronger complexation and bridging effects of Ca^{2+} compared to Mg^{2+} (Philippe and Schaumann, 2014). In contrast to Ca^{2+} and Mg^{2+}, the presence of Na^{+} at concentrations between 1 and 100 mM had a minimal effect on the formation and aggregation of HA-Cr(III) colloids (Fig. 4c and d) due to the high negative charge of the suspensions (<−35 mV, Fig. S3).

3.4. Characterization of NOM-Cr(III) colloids

High resolution Cs-STEM provided nanoscale information on the morphology and microscopic structure of HA-Cr(III) colloids formed at pH 6 (Fig. 5). The high-angle annular dark field (HAADF)-STEM images showed that the colloidal particles for both AHA-Cr and PPSHA-Cr samples exhibited irregular morphology with average primary diameters between 5 and 50 nm (Fig. 5a and b). The fast Fourier transform (FFT) patterns (the insets in Fig. 5a and b) showed no obvious lattice fringes for both HA-Cr(III) colloids, indicative of poor crystallinity or amorphous materials. HAADF-STEM-EDS mappings showed similar elemental distribution of C and Cr across the imaged regions (Fig. 5), indicating the intimate association of HA with Cr at the nanoscale. As the electron intensity of HAADF-STEM imaging is approximately proportional to the atomic number (Pennycook and Nellist, 2011), the brighter spots in HAADF images must correspond to Cr given that Cr has a larger atomic number compared to C (24 versus 6) (Fig. 5). EDS mappings confirmed this proposition, showing that C was either homogenously or heterogeneously enriched on the surface of electron-dense areas that were likely composed of HA-Cr nanoparticles or cluster (Fig. 5). Further evidence in support of this conclusion is provided below.

XPS spectroscopy was used to further characterize the chemical state and distribution of Cr present on the particle (near) surface (Fig. 6a–c). Spectra of Cr(III) (as $CrCl_3$ solid) and Cr(VI) (as $K_2Cr_2O_7$ solid) were provided as references for comparison. Consistent with the findings of aqueous phase analysis as discussed above, the Cr 2p XPS spectra of solids from reaction of Cr(VI) with HA_{red} (both AHA_{red} and $PPSHA_{red}$) at pH 6 revealed that Cr(VI) was completely reduced to Cr(III) as there was no significant Cr(VI) feature peak (e.g., ~579.6 eV) (Fig. 6a). Fitting the high-resolution Cr 2p 3/2 spectra further confirmed the domination of Cr(III) on the particle near surface (Fig. 6a), which is consistent with prior X-ray absorption near edge structure spectroscopy (XANES) measurements that showed that the solid products of Cr(VI) reduction by HA material contained solely Cr(III) (Jiang et al., 2014). Because XPS typically probes the topmost 1–10 nm of samples, we then performed a XPS depth profiling technique to probe the spatial distribution of Cr as a function of probing depth (from surface to 100 nm depth) (Fig. 6b and c). Results indicated that Cr(III) dominated at all depths tested, and the intensity of Cr(III) increased with increasing probing depth for both AHA-Cr and PPSHA-Cr samples (Fig. 6b and c), suggesting the relative enrichment of HA on the surface of HA-Cr(III) colloids. This is consistent with the HAADF-STEM-EDS results described above (Fig. 5). The HA rich surface could explain the high colloidal stability of HA-Cr(III) particles observed under our experimental conditions.

ATR-FTIR spectroscopy provided molecular information on the binding of HA with reduced Cr(III) for colloidal HA-Cr(III) complex formation (Fig. 6d). The spectra of samples from the reaction of HA_{red} with Cr(VI) were much different from the initial unreacted HA_{red}. The two broad peaks at 1596 and 1391 cm^{-1} in the unreacted HA_{red} suggest asymmetric and symmetric vibrations for COO^{-} groups (Sharma et al., 2010). After completion of Cr(VI) reduction, the asymmetric COO^{-} peak at 1596 cm^{-1} shifted to a higher wavenumber of 1636 cm^{-1}, and the intensity of this peak decreased for both AHA-Cr and PPSHA-Cr samples (Fig. 6d). Such a large shift and decrease in the intensity of COO^{-} stretching band is likely attributed to the formation of carboxylate-metal bonds through a ligand exchange mechanism (Sharma et al., 2010; Chen et al., 2014). In addition, the spectra for samples after reactions resulted in a significant decrease in the intensity of a symmetric COO^{-} peak at 1400 cm^{-1} (Fig. 6d), further suggesting that carboxyl groups were involved in the complexation of HA with reduced Cr(III). These observations are consistent with recent extended X-ray absorption fine structure spectroscopy (EXAFS) results showing that Cr(III) formed stable polynuclear complexes with NOM at pH > 5 primarily through carboxyl functional groups (Gustafsson et al., 2014). Further, the broad new peaks at 1205 and 1113 cm^{-1} after reactions may be attributed to the Cr–O–C bridge vibrations or Cr–OH stretching vibration (Nakamoto, 1978). The shape of the spectra for both AHA-Cr and PPSHA-Cr samples were similar, but AHA-Cr sample yielded a higher peak intensity at 1205 and 1113 cm^{-1} (Fig. 6d).

3.5. Environmental implications

Redox transformation of NOM_{ox} to NOM_{red} by microorganisms or geochemical reductants occurs ubiquitously in anoxic environments (Lovley et al., 1996; Gu et al., 2011; Liao et al., 2017b), and the interplays between NOM_{red} and Cr(VI) are of particular importance for better understanding of Cr speciation and mobility in subsurface environments. This study extended our fundamental knowledge of the interaction of NOM with Cr(VI) from oxic conditions to anoxic conditions, and provided clear evidence that NOM_{red} exerts an important control on the reduction of Cr(VI) and stabilization of colloidal Cr(III) particles under anoxic conditions. Such complex Cr cycles triggered by NOM_{red} are likely widespread in anoxic

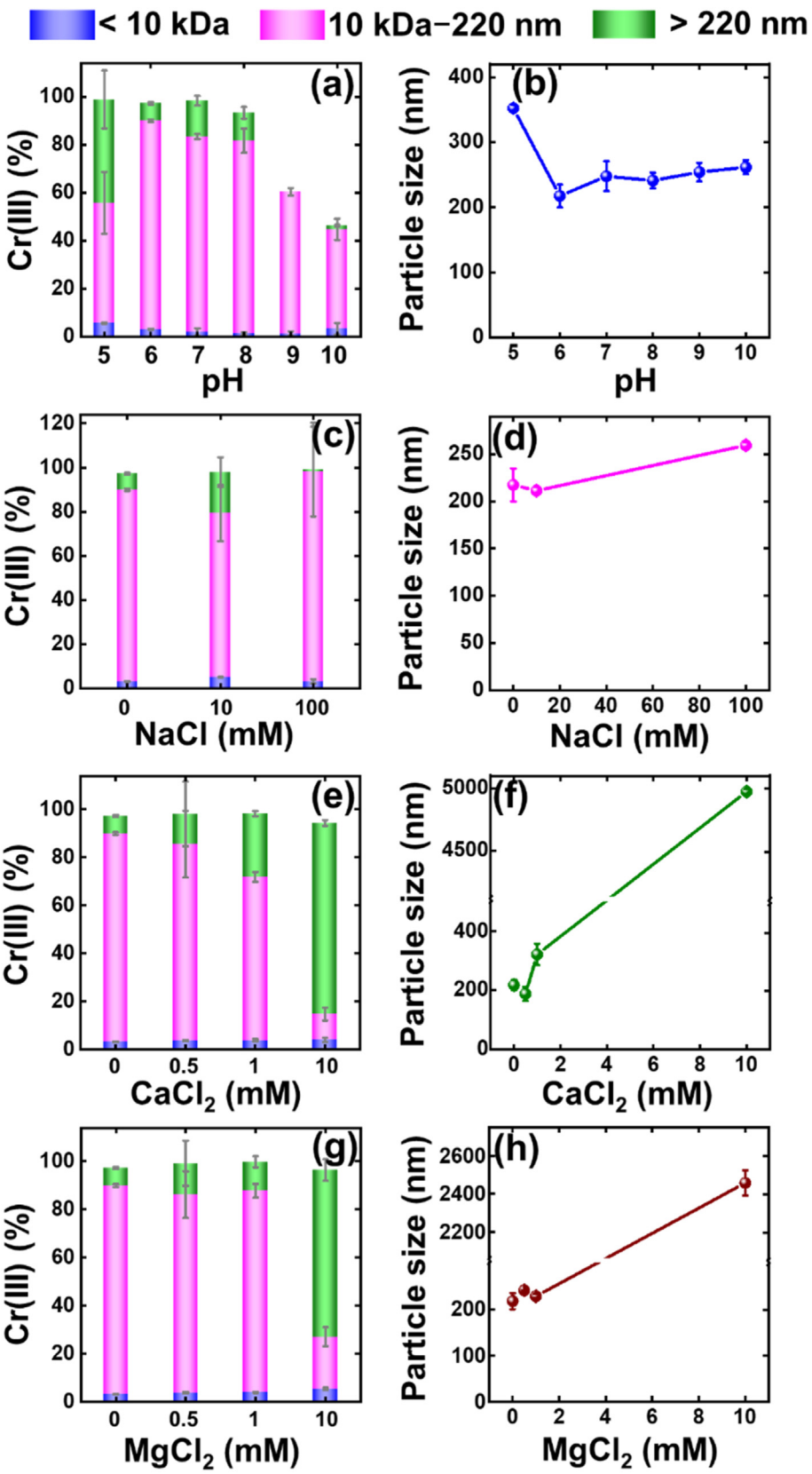

Fig. 4. (a,c,e,g) Effect of (a) pH, (c) Na^{+}, (e) Ca^{2+}, and (g) Mg^{2+} concentrations on the percentage of Cr(III) concentrations after Cr(VI) reduction in different size fractions under anoxic steady-state conditions. The AHA_{red} concentration was fixed at 40 mg C/L. The percentage in y-axis represents the concentration of Cr(III) in a certain size fraction to the total concentration of Cr in the suspension. (b,d,f,h) Effect of (b) pH, (d) Na^{+}, (f) Ca^{2+}, and (h) Mg^{2+} concentrations on the Z-averaged hydrodynamic diameter of HA-Cr suspensions after Cr(VI) reduction under anoxic steady-state conditions. Error bars represent the standard deviations of at least duplicate measurements.

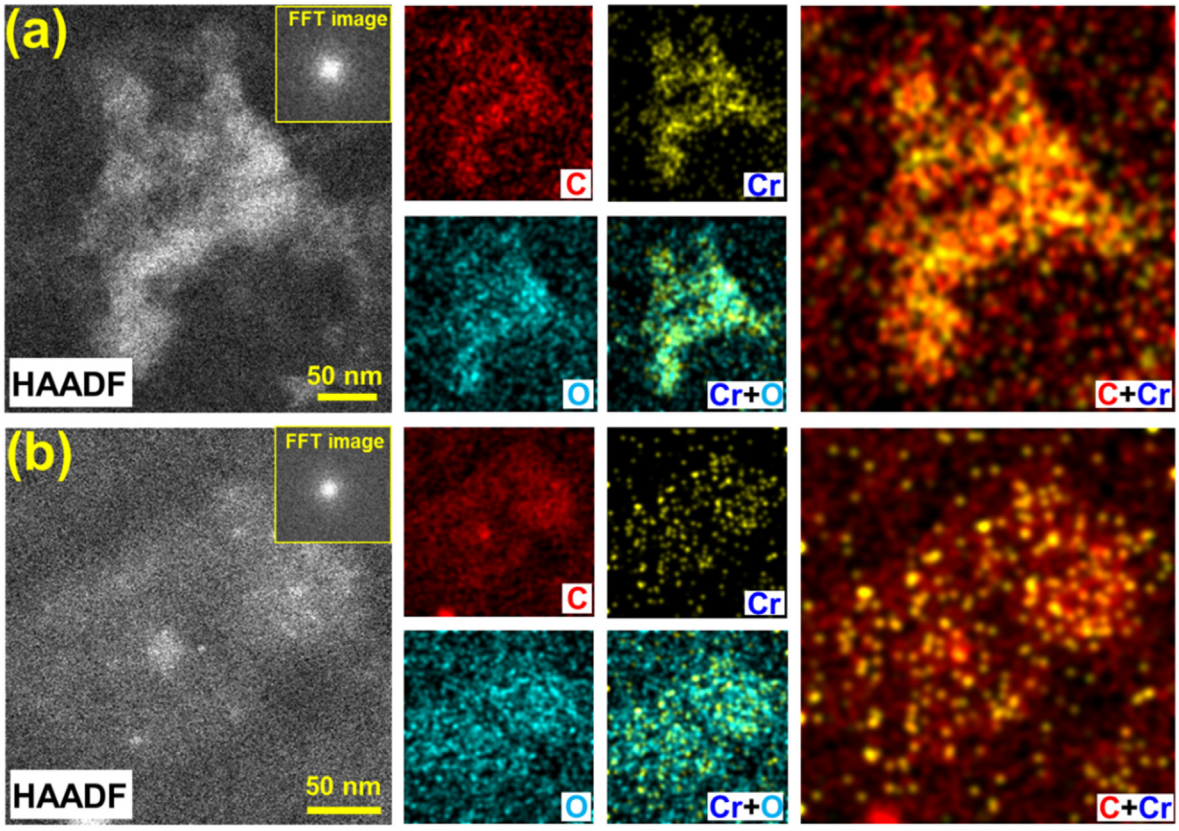

Fig. 5. High-resolution HAADF-STEM images and the corresponding EDS elemental mapping images of (a) AHA-Cr and (b) PPSHA-Cr suspensions after Cr(VI) reduction under anoxic steady-state conditions at pH 6. HAADF-STEM images and EDS mappings displayed were representative of typical images collected for each sample. All images were taken at a comparable magnification of scale bar of 50 nm.

geochemical conditions and suggest that the fate and transport of Cr may be more complicated than previously recognized. As expected, Cr(VI) that is diffused from oxic zones across oxic-anoxic transition interfaces into anoxic environments can be quickly reduced by NOM_{red}. Rates of Cr(VI) reduction by NOM_{red} (Table S2) are considerably faster than those observed for microbial Cr(VI) reduction pathways (e.g., 3.81–8.95 $\times$ 10^{-3} min^{-1}) in anoxic subsurface environments (Gu and Chen, 2003; Liu et al., 2002). Although Cr(VI) reduction by NOM has been posited as a sink for Cr (Wittbrodt and Palmer, 1995; Jiang et al., 2014), the reduced Cr(III) produced at lower Ca^{2+} and Mg^{2+} concentrations is resistant to precipitate due to the formation of stable NOM-Cr(III) colloids, which are composed of small particles that stayed suspended in water for months. Such high colloidal stability highlights that colloid-facilitated transport of Cr(III) particles may be a significant process governing the mobility of Cr in subsurface. Given the dynamic redox nature of subsurface environments, transport of NOM-Cr(III) colloids from anoxic environments across interfaces and into more oxygenated zones could enhance the probability of future reoxidation of Cr(III) to toxic, highly mobile Cr(VI) by oxidants such as manganese oxides and chloramine disinfectants (Landrot et al., 2012; Chebeir and Liu, 2016; Pan et al., 2017b; Liao et al., 2020), thereby spreading contamination. However, NOM-Cr(III) colloids could be aggregated and destabilized by the presence of higher Ca^{2+} and Mg^{2+} concentrations, thus promoting Cr(III) removal from the water column. Since organically complexed Cr(III) represents an important part of the biogeochemical cycle of Cr (Puzon et al., 2005), we proposed that colloid-facilitated Cr(III) transport needs to be considered within the overall theoretical framework for reactive transport of Cr under organic-rich redox dynamic conditions. Further work is needed to extend our framework by deciphering the aggregation, deposition, transport, and transformation of NOM-Cr(III) colloids in more realistic subsurface environments.

4. Conclusions

This study, to our knowledge, is the first report elucidating HA_{red}-mediated Cr(VI) reduction mechanism and colloidal stability of reduced Cr(III) products under circumneutral anoxic conditions. The most striking observation is that HA_{red} triggered rapid reduction of Cr(VI) and formation of stable organic-Cr(III) colloids over a wide range of anoxic conditions. Specifically, the reduced quinone moieties present in HA_{red} can quickly transfer electrons to Cr(VI), with Cr(VI) reduction occurring on the time scale of minutes at neutral pH conditions (6–8). The presence of Na^{+} (1–100 mM), Ca^{2+} (0.5–10 mM), and Mg^{2+} (0.5–10 mM) enhanced Cr(VI) reduction at pH 6. Reduced Cr(III) can then complex with carboxyl groups of HA to form stable HA-Cr(III) colloids that persisted in water for at least 2 months with negligible aggregation due to strong electrostatic interactions between particles. However, the presence of Ca^{2+} and Mg^{2+} at higher concentrations (e.g., 10 mM) promoted particle aggregation and thus suppressed HA-Cr(III) colloid formation. Taken together, our results provided new insights into the understanding of the fate and transport of Cr in organic-rich anoxic environments, which is also critical for evaluating the long-term efficiency of subsurface Cr(VI) remediation strategies.

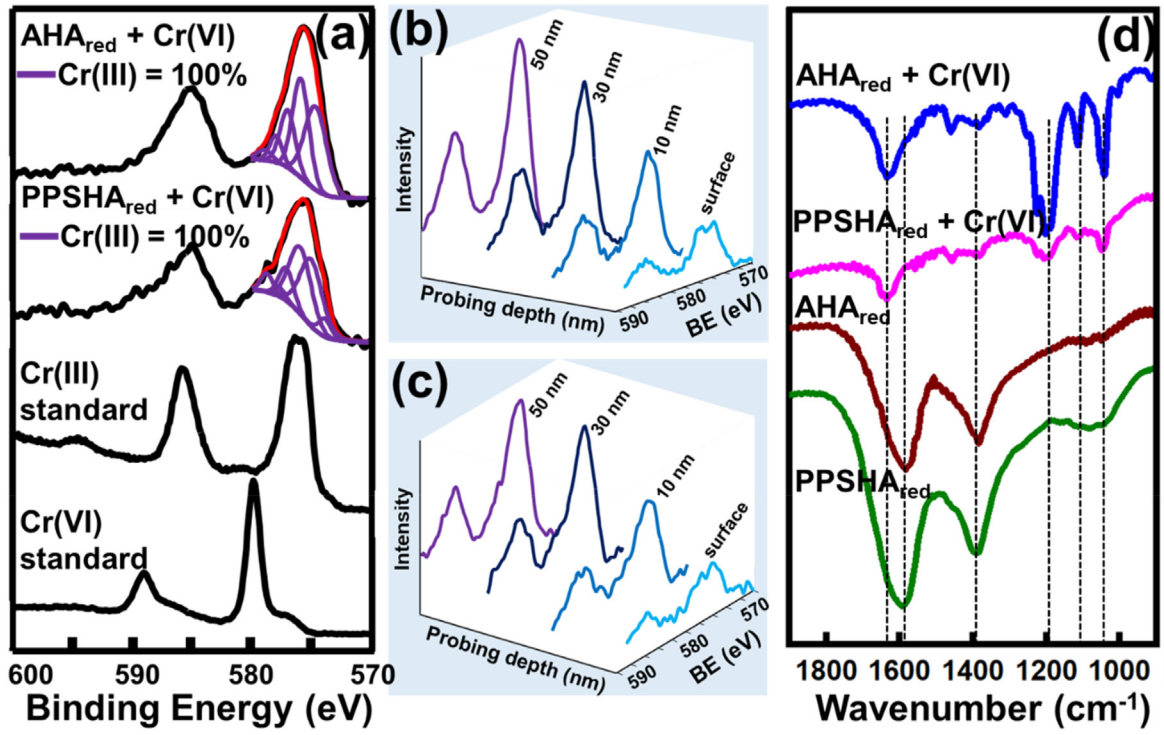

Fig. 6. (a) XPS Cr 2p narrow region spectra and curve-fitting analysis of Cr-HA solids collected from the end of batch Cr(VI) reduction experiments under anoxic steady-state conditions at pH 6. All spectra were collected at the XPS probing depth of 50 nm. Peak fitting was performed only for the Cr $2p_{3/2}$ peak. For reference, the patterns of $CrCl_3$ and $K_2Cr_2O_7$ were included in the XPS plots. (b,c) XPS depth profiling spectra (Cr 2p) of (b) AHA-Cr and (c) PPSHA-Cr solids collected after Cr(VI) reduction under anoxic conditions at pH 6. (d) ATR-FTIR spectra of Cr-HA solids collected after Cr(VI) reduction under anoxic conditions at pH 6. Both XPS and ATR-FTIR analysis of solid samples were obtained at a fixed initial AHA_{red} of 80 mg C/L and $PPSHA_{red}$ of 150 mg C/L.

Declaration of competing interest

The authors declare that they have no known competing financial interests or personal relationships that could have appeared to influence the work reported in this paper.

Acknowledgments

This study was supported by the National Natural Science Foundation of China (No. 41703128) and the Program for Guangdong Introducing Innovative and Entrepreneurial Teams (2017ZT07Z479). HAADF-STEM-EDS measurements were performed at the Pico Center at Southern University of Science and Technology.

Appendix A. Supplementary data

Supplementary data to this article can be found online at https://doi.org/10.1016/j.watres.2020.115923.

References

Aeschbacher, M., Sander, M., Schwarzenbach, R.P., 2010. Novel electrochemical approach to assess the redox properties of humic substances. Environ. Sci. Technol. 44, 87–93.
Aiken, G., McKnight, D., Wershaw, R., MacCarthy, P., 1985. Humic Substances in Soil, Sediment, and Water: Geochemistry, Isolation and Characterization. John Wiley & Sons, New York.
Aiken, G.R., Hsu-Kim, H., Ryan, J.N., 2011. Influence of dissolved organic matter on the environmental fate of metals, nanoparticles, and colloids. Environ. Sci. Technol. 45, 3196–3201.
Bauer, I., Kappler, A., 2009. Rates and extent of reduction of Fe(III) compounds and O_2 by humic substances. Environ. Sci. Technol. 43, 4902–4908.
Blowes, D., 2002. Tracking hexavalent Cr in groundwater. Science 295, 2024–2025.
Buerge, I.J., Hug, S.J., 1998. Influence of organic ligands on chromium(VI) reduction by iron(II). Environ. Sci. Technol. 32, 2092–2099.
Chebeir, M., Liu, H.Z., 2016. Kinetics and mechanisms of Cr(VI) formation via the oxidation of Cr(III) solid phases by chlorine in drinking water. Environ. Sci. Technol. 50, 701–710.
Chen, C., Dynes, J., Wang, J., Sparks, D.L., 2014. Properties of Fe organic matter associations via coprecipitation versus adsorption. Environ. Sci. Technol. 48, 13751–13759.
Coates, J.D., Ellis, D.J., Blunt-Harris, E.L., Gaw, C.V., Roden, E.E., Lovley, D.R., 1998. Recovery of humic-reducing bacteria from a diversity of environments. Appl. Environ. Microbiol. 64, 1504–1509.
Eary, L.E., Rai, D., 1988. Chromate removal from aqueous wastes by reduction with ferrous iron. Environ. Sci. Technol. 22 (8), 972–977.
Elimelech, M., Gregory, J., Jia, X., Williams, R., 1995. Particle Deposition and Aggregation: Measurement, Modelling and Simulation. Butterworth-Heinemann, Woburn, MA.
Fendorf, S.E., Li, G., 1996. Kinetics of chromate reduction by ferrous iron. Environ. Sci. Technol. 30, 1614–1617.
Fukushima, M., Nakayasu, K., Tanaka, S., Nakamura, H., 1995. Chromium (III) binding abilities of humic acids. Anal. Chim. Acta 317, 195–206.
Graham, A.M., Bouwer, E.J., 2010. Rates of hexavalent chromium reduction in anoxic estuarine sediments: pH effects and the role of acid volatile sulfides. Environ. Sci. Technol. 44, 136–142.
Gu, B., Chen, J., 2003. Enhanced microbial reduction of Cr(VI) and U(VI) by different natural organic matter fractions. Geochem. Cosmochim. Acta 67, 3575–3582.
Gu, B.H., Bian, Y.R., Miller, C.L., Dong, W.M., Jiang, X., Liang, L.Y., 2011. Mercury reduction and complexation by natural organic matter in anoxic environments. Proc. Natl. Acad. Sci. U.S.A. 108, 1479–1483.
Gustafsson, J.P., Persson, I., Oromieh, A.G., van Schaik, J.W.J., Sjöstedt, C., Kleja, D.B., 2014. Chromium(III) complexation to natural organic matter: mechanisms and modeling. Environ. Sci. Technol. 48, 1753–1761.
Hering, J.G., Morel, F.M.M., 1988. Kinetics of trace metal complexation: role of alkaline-earth metals. Environ. Sci. Technol. 22, 1469–1478.
Hu, L., Cai, Y., Jiang, G., 2016. Occurrence and speciation of polymeric chromium(III), monomeric chromium(III) and chromium(VI) in environmental samples. Chemosphere 156, 14–20.
Icopini, G.A., Long, D.T., 2002. Speciation of aqueous chromium by use of solid-phase extractions in the field. Environ. Sci. Technol. 36, 2994–2999.
James, B.R., Bartlett, R.J., 1983. Behavior of chromium in soils. 5. Fate of organically complexed Cr(III) added to soil. J. Environ. Qual. 12, 169–172.
Jiang, J., Kappler, A., 2008. Kinetics of microbial and chemical reduction of humic substances: implications for electron shuttling. Environ. Sci. Technol. 42,

3563–3569.
Jiang, W.J., Cai, Q., Xu, W., Yang, M.W., Cai, Y., Dionysiou, D.D., O'Shea, K.E., 2014. Cr(VI) adsorption and reduction by humic acid coated on magnetite. Environ. Sci. Technol. 48, 8078–8085.
Kaczynski, S.E., Kieber, R.J., 1994. Hydrophobic C18 bound organic complexes of chromium and their potential impact on the geochemistry of chromium in natural waters. Environ. Sci. Technol. 28, 799–804.
Kappler, A., Haderlein, S.B., 2003. Natural organic matter as reductant for chlorinated aliphatic pollutants. Environ. Sci. Technol. 37, 2714–2719.
Landrot, G., Ginder-Vogel, M., Livi, K.J.T., Fitts, J.P., Sparks, D.L., 2012. Chromium(III) oxidation by three poorly-crystalline manganese-(IV) oxides 1. Chromium (III)-oxidizing capacity. Environ. Sci. Technol. 46, 11594–11600.
Li, Q.Q., Xie, L., Jiang, Y., Fortner, J.D., Yu, K., Liao, P., Liu, C.X., 2019. Formation and stability of NOM-Mn(III) colloids in aquatic environments. Water Res. 149, 190–201.
Lian, J., Li, Z.F., Xu, Z.F., Guo, J.B., Hu, Z.Z., Guo, Y.K., Li, M., Yang, J.L., 2016. Isolation and Cr(VI) reduction characteristics of quinone respiration in Mangrovibacter plantisponsor strain CR1. Biotechnol. Appl. Biochem. 63, 595–600.
Liao, P., Li, W.L., Jiang, Y., Wu, J., Yuan, S.H., Fortner, J.D., Giammar, D.E., 2017a. Formation, aggregation, and deposition dynamics of NOM-Iron colloids at anoxic-oxic interfaces. Environ. Sci. Technol. 51, 12235–12245.
Liao, P., Li, W.L., Wang, D.G., Jiang, Y., Pan, C., Fortner, J.D., Yuan, S.H., 2017b. Effect of reduced humic acid on the transport of ferrihydrite nanoparticles under anoxic conditions. Water Res. 109, 347–357.
Liao, P., Liang, Y.Z., Shi, Z.H., 2019. Impact of divalent cations on dark production of hydroxyl radicals from oxygenation of reduced humic acids at anoxic-oxic interfaces. ACS Earth Space Chem. 3, 484–494, 2019.
Liao, P., Pan, C., Ding, W.Y., Li, W.L., Yuan, S.H., Fortner, J.D., Giammar, D.E., 2020. Formation and transport of Cr(III)-NOM-Fe colloids upon reaction of Cr(VI) with NOM-Fe(II) colloids at anoxic-oxic interfaces. Environ. Sci. Technol. 54, 4256–4266.
Lide, D.R., 2000. Handbook of Chemistry and Physics, 81st ed. CRC Press.
Liu, C., Gorby, Y.A., Zachara, J.M., Fredrickson, J.K., Brown, C.F., 2002. Reduction kinetics of Fe(III), Co(III), U(VI), Cr(VI), and Tc(VII) in cultures of dissimilatory metal reducing Bacteria. Biotechnol. Bioeng. 80, 637–649.
Liu, G.L., Fernandez, A., Cai, Y., 2011. Complexation of arsenite with humic acid in the presence of ferric iron. Environ. Sci. Technol. 45, 3210–3216.
Liu, Y.Y., Xu, F., Liu, C.X., 2017. Coupled hydro-biogeochemical processes controlling Cr reductive immobilization in Columbia river hyporheic zone. Environ. Sci. Technol. 51, 1508–1517.
Lovley, D.R., Coates, J.D., Blunt-Harris, E.L., Phillips, E.J.P., Woodward, J.C., 1996. Humic substances as electron acceptors for microbial respiration. Nature 382, 445–448.
Lovley, D.R., Blunt-Harris, E.L., 1999. Role of humic-bound iron as an electron transfer agent in dissimilatory Fe(III) reduction. Appl. Environ. Microbiol. 65, 4252–4254.
Lovley, D.R., Anderson, R.T., 2000. Influence of dissimilatory metal reduction on the fate of organic and metal contaminants in the subsurface. Hydrogeol. J. 8, 77–88.
McClain, C.N., Fendorf, S., Webb, S.M., Maher, K., 2017. Quantifying Cr(VI) production and export from serpentine soil of the California coast range. Environ. Sci. Technol. 51, 141–149.
McNeill, L., McLean, J., Edwards, M., Parks, J., 2012. State of the Science of Hexavalent Chromium in Drinking Water. Water Research Foundation, Denver, pp. 1–36.
Nakamoto, K., 1978. Infrared and Raman Spectra of Inorganic and Coordination Compounds, third ed. John Wiley, New York.
Nakayasu, K., Fukushima, M., Sasaki, K., Tanaka, S., Nakamura, H., 1999. Comparative studies of the reduction behavior of chromium-(VI) by humic substances and their precursors. Environ. Toxicol. Chem. 18, 1085–1090.
Pan, C., Troyer, L.D., Catalano, J.G., Giammar, D.E., 2016. Dynamics of chromium(VI) removal from drinking water by iron electrocoagulation. Environ. Sci. Technol. 50, 13502–13510.
Pan, C., Troyer, L.D., Liao, P., Catalano, J.G., Li, W., Giammar, D.E., 2017a. Effect of humic acid on the removal of chromium(VI) and the production of solids in iron electrocoagulation. Environ. Sci. Technol. 51, 6308–6318.
Pan, C., Liu, H., Catalano, J.G., Qian, A., Wang, Z.M., Giammar, D.E., 2017b. Rates of Cr(VI) generation from $Cr_xFe_{1-x}(OH)_3$ solids upon reaction with manganese oxide. Environ. Sci. Technol. 51, 12416–12423.
Patterson, R.R., Fendorf, S., Fendorf, M., 1997. Reduction of hexavalent chromium by amorphous iron sulfide. Environ. Sci. Technol. 31, 2039–2044.
Pennycook, S.J., Nellist, P.D., 2011. Scanning Transmission Electron Microscopy: Imaging and Analysis. Springer.
Philippe, A., Schaumann, G.E., 2014. Interactions of dissolved organic matter with natural and engineered inorganic colloids: a review. Environ. Sci. Technol. 48, 8946–8962.
Pokrovsky, O.S., Schott, J., 2002. Iron colloids/organic matter associated transport of major and trace elements in small boreal rivers and their estuaries (NW Russia). Chem. Geol. 190, 141–179.
Puzon, G.J., Roberts, A.G., Kramer, D.M., Xun, L., 2005. Formation of soluble organo-chromium(III) complexes after chromate reduction in the presence of cellular organics. Environ. Sci. Technol. 39, 2811–2817.
Puzon, G.J., Tokala, R.K., Zhang, H., Yonge, D., Peyton, B.M., Xun, L., 2008. Mobility and recalcitrance of organo-chromium(III) complexes. Chemosphere 70, 2054–2059.
Ratasuk, N., Nanny, M.A., 2007. Characterization and quantification of reversible redox sites in humic substances. Environ. Sci. Technol. 41, 7844–7850.
Richard, F.C., Bourg, A.C.M., 1991. Aqueous geochemistry of chromium: a review. Water Res. 25, 807–816.
Sander, S.G., Koschinsky, A., 2011. Metal flux from hydrothermal vents increased by organic complexation. Nat. Geosci. 4, 145–150.
Sass, B.M., Rai, D., 1987. Solubility of amorphous chromium(III)-iron(III) hydroxide solid solutions. Inorg. Chem. 26, 2228–2232.
Scott, D.T., McKnight, D.M., Blunt-Harris, E.L., Kolesar, S.E., Lovley, D.R., 1998. Quinone moieties act as electron acceptors in the reduction of humic substances by humic-reducing microorganisms. Environ. Sci. Technol. 32, 2984–2989.
Sharma, P., Ofner, J., Kappler, A., 2010. Formation of binary and ternary colloids and dissolved complexes of organic matter, Fe and as. Environ. Sci. Technol. 44, 4479–4485.
Stevenson, F.J., 1994. Humus Chemistry: Genesis, Composition, Reactions, second ed. John Wiley & Sons, New York.
Tamura, H., Goto, K., Yotsuyanagi, T., Nagayama, M., 1974. Spectrophotometric determination of iron (II) with 1, 10-phenanthroline in the presence of large amounts of iron (III). Talanta 21, 314–318.
Wadhawan, A.R., Stone, A.T., Bouwer, E.J., 2013. Biogeochemical controls on hexavalent chromium formation in estuarine sediments. Environ. Sci. Technol. 47, 8220–8228.
Wall, N.A., Choppin, G.R., 2003. Humic acids coagulation: influence of divalent cations. Appl. Geochem. 18, 1573–1582.
Wittbrodt, P.R., Palmer, C.D., 1995. Reduction of Cr(VI) in the presence of excess soil fulvic acid. Environ. Sci. Technol. 29, 255–263.
Wittbrodt, P.R., Palmer, C.D., 1996. Effect of temperature, ionic strength, background electrolytes, and Fe(III) on the reduction of hexavalent chromium by soil humic substances. Environ. Sci. Technol. 30, 2470–2477.
Wu, J.F., Boyle, E., Sunda, W., Wen, L.S., 2001. Soluble and colloidal iron in the oligotrophic North Atlantic and North Pacific. Science 293, 847–849.
Zheng, W., Liang, L.Y., Gu, B.H., 2012. Mercury reduction and oxidation by reduced natural organic matter in anoxic environments. Environ. Sci. Technol. 46, 292–299.